

1  
2

## JAST (Journal of Animal Science and Technology) TITLE PAGE

ARTICLE INFORMATION	Fill in information in each box below
<b>Article Type</b>	Research article
<b>Article Title (within 20 words without abbreviations)</b>	<i>Aporocactus flagelliformis</i> water extract and limonin suppresses P2Y <sub>14</sub> purinoceptor 14-mediated proinflammatory features in 3D4/31 porcine alveolar macrophages
<b>Running Title (within 10 words)</b>	AFWE and limonin suppresses P2Y <sub>14</sub> -mediated inflammation in porcine alveolar macrophages
<b>Author</b>	Hyungkuen Kim <sup>1</sup> , Hyun Sik Jun <sup>2</sup> , Ki-Duk Song <sup>3</sup> , Sung-Jo Kim <sup>1</sup>
<b>Affiliation</b>	1 Department of Biotechnology, College of Life and Health Sciences, Hoseo University, Asan, Korea 2 Department of Biotechnology and Bioinformatics, College of Science and Technology, Korea University, Sejong, Republic of Korea 3 Department of Agricultural Convergence Technology, Jeonbuk National University, Jeonju 54896, Korea
<b>ORCID (for more information, please visit <a href="https://orcid.org">https://orcid.org</a>)</b>	Hyungkuen Kim ( <a href="https://orcid.org/0000-0001-7508-9933">https://orcid.org/0000-0001-7508-9933</a> ) Hyun Sik Jun ( <a href="https://orcid.org/0000-0002-1570-7784">https://orcid.org/0000-0002-1570-7784</a> ) Ki-Duk Song ( <a href="https://orcid.org/0000-0003-2827-0873">https://orcid.org/0000-0003-2827-0873</a> ) Sung-Jo Kim ( <a href="https://orcid.org/0000-0003-4590-3644">https://orcid.org/0000-0003-4590-3644</a> )
<b>Email address</b>	Hyungkuen Kim (20205284@vision.hoseo.edu) Hyun Sik Jun (toddjun@korea.ac.kr) Ki-Duk Song (kiduk.song@jbnu.ac.kr) Sung-Jo Kim (sungjo@hoseo.edu)
<b>Competing interests</b>	No potential conflict of interest relevant to this article was reported.
<b>Funding sources</b> State funding sources (grants, funding sources, equipment, and supplies). Include name and number of grant if available.	This work was supported by the Basic Science Research Program through the National Research Foundation of Korea (NRF) funded by the Ministry of Education(2021R1F1A1049562); and the 'R&D Program for Forest Science Technology (2021374C10-2123-BD02)' provided by the Korea Forest Service (Korea Forestry Promotion Institute).
<b>Acknowledgements</b>	Not applicable.
<b>Availability of data and material</b>	Upon reasonable request, the datasets of this study can be available from the corresponding author.
<b>Authors' contributions</b> Please specify the authors' role using this form.	Conceptualization: Kim H, Jun HS, Song KD, Kim SJ. Methodology: Kim H. Investigation: Kim H. Writing - original draft: Kim H. Writing - review & editing: Jun HS, Song KD, Kim SJ.
<b>Ethics approval and consent to participate</b>	This article does not require IRB/IACUC approval because there are no human and animal participants.

3  
4

5 **CORRESPONDING AUTHOR CONTACT INFORMATION**

<b>For the corresponding author (responsible for correspondence, proofreading, and reprints)</b>	<b>Fill in information in each box below</b>
First name, middle initial, last name	Ki-Duk Song
Email address – this is where your proofs will be sent	kiduk.song@jbnu.ac.kr
Secondary Email address	kiduk.song@gmail.com
Address	567 Baek-jedaero, Deokjin gu, Jeonju, Korea
Cell phone number	+82-10-5622-1158
Office phone number	+82-63-219-5523
Fax number	+82-63-270-4739

6

7

<b>For the corresponding author (responsible for correspondence, proofreading, and reprints)</b>	<b>Fill in information in each box below</b>
First name, middle initial, last name	Sung-Jo, Kim
Email address – this is where your proofs will be sent	sungjo@hoseo.edu
Secondary Email address	sungjo@gmail.com
Address	Hoseo University, Baebang, Asan 31499, Korea
Cell phone number	+82-10-7268-9981
Office phone number	+82-41-540-5571
Fax number	+82-41-540-5898

8

9

## Abstract

10

11 Respiratory diseases have been recognized as a significant cause of reduced livestock productivity since 1995.  
12 Respiratory diseases in the swine industry caused by both biological and non-biological factors are collectively  
13 referred to as porcine respiratory disease complex (PRDC). However, there is a lack of eco-friendly anti-inflammatory  
14 drugs (AIDs) that can effectively control lung inflammation caused by PRDC. P2Y purinoreceptor 14 (P2Y<sub>14</sub>) has  
15 been identified as a key regulator of macrophage inflammatory responses; however, its regulatory role in porcine lung  
16 inflammation remains unclear. In this study, we investigated the role of P2Y<sub>14</sub> in inflammation in 3D4/31 PAMs and  
17 attempted to develop a novel AID. An extract of the Mexican medicinal plant *Aporocactus flagelliformis* (AFWE)  
18 reduced ROS production and pro-inflammatory cytokine expression in phorbol myristate acetate-stimulated 3D4/31-  
19 PAMs. It also reduced glucose uptake, glycogen accumulation, and expression of genes related to the P2Y<sub>14</sub> cascade.  
20 Polarity-based fractionation and liquid chromatography-mass spectrometry identified limonin as an anti-inflammatory  
21 compound in AFWE. Limonin reduced P2RY14 and proinflammatory gene expression induced by the P2Y<sub>14</sub> ligand  
22 UDPG in 3D4/31-PAMs, demonstrating its inhibitory effect on P2Y<sub>14</sub>-mediated inflammation. These results suggest  
23 that P2Y<sub>14</sub> is an inflammatory receptor in PAMs and an effective target for AID development. We also propose AFWE  
24 and limonin as candidate AIDs for pigs.

25

26 **Keywords:** Porcine respiratory disease complex, Porcine alveolar macrophages, inflammation, P2Y<sub>14</sub>, *Aporocactus*  
27 *flagelliformis*, limonin

28

29

## INTRODUCTION

30 The porcine respiratory disease complex (PRDC) causes economic losses in the swine industry by reducing pork  
31 production efficiency and increasing feed costs, carcass disposal costs, and medical expenses [1]. Various factors,  
32 including overcrowded rearing conditions, porcine circovirus type 2 (PCV2), porcine reproductive and respiratory  
33 syndrome virus, swine influenza virus, *Mycoplasma hyopneumoniae*, and *Pasteurella multocida* influence the onset  
34 of PRDC [2]. Infections by PRDC-related viruses lead to proinflammatory cytokine expression and tissue damage in  
35 porcine lungs [3], which can be alleviated by anti-inflammatory drugs (AIDs). However, the development and  
36 selection of suitable AIDs for PRDC are limited because of a lack of research [4]. Therefore, in this study, we aimed  
37 to develop an AID for porcine.

38 Inflammation caused by infection is primarily mediated by macrophages. PCV2 targets macrophage populations,  
39 including alveolar macrophages (AMs), and induces a strong inflammatory response [5]. Increased expression of  
40 NOX2, which mediates reactive oxygen species (ROS) production, has been reported in PCV2-infected macrophages  
41 [6]. This induces autophagy and PCV2 replication, which can be inhibited by blocking autophagy or ROS [7, 8].  
42 Additionally, PCV2-infected macrophages show increased expression of proinflammatory cytokines, including tumor  
43 necrosis factor- $\alpha$  (TNF $\alpha$ ) and cyclooxygenase-2 (COX2) [9]. The acute inflammatory response in macrophages is  
44 mediated by P2Y purinoceptor 14 (P2Y<sub>14</sub>), which is a member of the pyrimidinergic G protein-coupled receptor family.  
45 Activation of P2Y<sub>14</sub> by uridine-5'-diphosphoglucose (UDPG), which is produced and secreted during glycogenesis,  
46 induces the expression of signal transducer and activator of transcription 1 (STAT1) and TNF $\alpha$  [10]. Although the  
47 ability of P2Y<sub>14</sub> to recognize UDPG has been reported in porcine coronary arteries [11], the role of P2Y<sub>14</sub> in porcine  
48 macrophages (PAMs) is unclear.

49 With the global ban on antibiotics in animal feed, there has been increased attention on developing eco-friendly  
50 antibacterial and anti-inflammatory strategies to maintain porcine health and productivity [12]. Succulent plants,  
51 which are also used as porcine feed, have shown some anti-inflammatory effects in porcine cells and are emerging as  
52 natural anti-inflammatory agents [13-15]. The succulent *Aporocactus flagelliformis* (*A. flagelliformis*), also known as  
53 rattail cactus, is traditionally used in Mexico to treat heart disease and diabetes [16, 17]. Inhibition of P2Y<sub>14</sub> in porcine  
54 shows potential for treating these conditions [11, 18]. Here, we focused on the therapeutic effects of *A. flagelliformis*  
55 on P2Y<sub>14</sub> and various diseases.

56 In this study, we developed an *A. flagelliformis* water extract (AFWE) and investigated its anti-inflammatory  
57 effects on 3D4/31-PAMs, including ROS production, proinflammatory cytokine expression, and bactericidal activity.

58 We also evaluated the effects of AFWE on P2Y<sub>14</sub> metabolism. Limonin was identified using liquid chromatography-  
59 mass spectrometry (LC-MS) as a major compound of AFWE. The binding potential of limonin to porcine P2Y<sub>14</sub> was  
60 assessed and the therapeutic effects of limonin on UDPG-induced inflammation were evaluated.

61

62

## 63 **MATERIALS AND METHODS**

### 64 **Preparation of *A. flagelliformis* water extract**

65 Fresh *A. flagelliformis* (Xplant, Seoul, Korea) was cut into 2-3 cm lengths, washed with deionized water (dH<sub>2</sub>O),  
66 and extracted with dH<sub>2</sub>O (300 mL dH<sub>2</sub>O for 100 g *A. flagelliformis*) for 15 min at 110 °C using a WAC-60 autoclave  
67 (Daihan Scientific, Wonju-si, Gangwon-do, Korea). The aqueous phase was collected, sterile filtered using a 0.2 µm  
68 cellulose-acetate filter (16534-K, Minisart, Sartorius, Goettingen, Germany), and stored at -80 °C before use.

69

### 70 **Cell culture condition**

71 3D4/31 porcine alveolar macrophages (3D4/31-PAMs; ATCC-CRL-2844; ATCC, Manassas, VA, USA) and  
72 A549 human alveolar epithelial cells (A549-AECs; CCL-185, ATCC) were maintained in a 5 % CO<sub>2</sub> atmosphere at  
73 36.5 °C. Cells were grown in a 4:6 ratio of Dulbecco's modified Eagle's medium (10-013-CVR, Corning, Corning,  
74 NY, USA) and Roswell Park Memorial Institute (RPMI) 1640 medium (10-040-CVR, Corning) supplemented with  
75 10 % (v/v) fetal bovine serum (TMS-013, Merck Millipore, Burlington, MA, USA) and 1 % (v/v) penicillin-  
76 streptomycin (LS202-02, Welgene, Gyeongsan-si, Gyeongsangbuk-do, Korea).

77

### 78 **Drugs and treatment**

79 Cells were cultured for 12 h prior to treatment. Cells were treated for 24 h, refreshed medium/treatment, and  
80 stimulated with 2 nM phorbol myristate acetate (PMA; P1585-1MG, Sigma-Aldrich, St. Louis, MO, USA). The  
81 treatments included 60 µg/mL AFWE, 30 µM limonin (A10531, Adooq Bioscience, Irvine, CA, USA), and 200 µM  
82 UDPG (U4625-25MG, Sigma-Aldrich). Limonin was prepared at a final concentration of 50 mM in 99.9 % dimethyl  
83 sulfoxide (DMSO; sterile, cell culture grade).

84

### 85 **Quantification of cell viability and proliferation**

86 To quantify cell viability, cells were cultured with 10 % (v/v) water-soluble tetrazolium salt-8 (WST8) reagent  
87 (QM2500, BIOMAX, Seoul, Korea) for 2 h, and the optical density at 450 nm ( $OD_{450}$ ) was measured using a FilterMax  
88 F3 microplate reader (Molecular Devices, San Jose, CA, USA). For quantification of proliferation, cells were  
89 harvested and stained with 0.2 % (v/v) trypan blue (15250-061, Gibco, North Andover, MA, USA) for 1 min, and  
90 viable cells were counted using a hemocytometer.

91

## 92 **Measurement of intracellular ROS level**

93 Cells were cultured with 1  $\mu$ M 2',7'-dichlorofluorescein diacetate ( $H_2DCFDA$ ; 35845, Sigma-Aldrich) for 30  
94 min, washed with phosphate-buffered saline (PBS; pH 7.4), harvested, washed with PBS, and analyzed by flow  
95 cytometry.

96

## 97 **Immunoblotting and densitometry analysis**

98 Cells were lysed in radioimmunoprecipitation assay buffer containing 1 mM phenylmethanesulfonyl fluoride  
99 (P7626-5G, Sigma-Aldrich) for 1 h at 4 °C. The supernatant was collected by centrifugation at 14,000 RCF for 15  
100 min. Protein concentration was quantified using Bradford's assay with a bovine serum albumin (BSA; 10735086001,  
101 Roche, Basel, Switzerland) standard. Proteins were separated by sodium dodecyl sulfate polyacrylamide gel  
102 electrophoresis and transferred onto polyvinylidene fluoride membranes (3010040001, Roche) using a HorizeBLOT  
103 2M transfer system (ATTO, Tokyo, Japan). Membranes were blocked with 5 % (w/v) skim milk, washed with tris-  
104 buffered saline [TBST; pH 7.6, 0.05 % (v/v) Tween 20], and probed with primary antibodies at 4 °C for 12 h.  
105 Membranes were then washed with TBST, probed with secondary antibodies, and washed with TBST. The membranes  
106 were then exposed to an enhanced chemiluminescence reagent, visualized using an X-ray film (EA8EC, AGFA,  
107 Mortsel, Belgium), and quantified by densitometry analysis using ImageJ Ver. 1.5.3q (National Institutes of Health,  
108 Bethesda, MD, USA). The antibodies used for immunoblotting are listed in Table 1.

109

## 110 **RNA isolation and quantitative real-time PCR (qRT-PCR)**

111 All procedures were performed according to the manufacturer's instructions. RNA was isolated using TRIzol  
112 reagent (15596026, Invitrogen, Carlsbad, CA, USA), quantified using NanoDrop, and converted to cDNA at a  
113 concentration of 1  $\mu$ g using Oligo dT20 primers with the WizScript cDNA Synthesis Kit (W2202, Wizbiosolutions,  
114 Seongnam-si, Gyeonggi-do, Korea). cDNA was quantified using SYBR Green qPCR Master Mix (DQ485; BioFACT,

115 Daejeon, Korea), StepOnePlus RT-PCR System (Applied Biosystems, Foster City, CA, USA), and StepOne software  
116 Ver. 2.3. The fold change in mRNA expression was normalized to *ribosomal protein S29 (RPS29)* using the  $2^{(-\Delta\Delta Ct)}$   
117 method. The primer sequences used for qRT-PCR are listed in Table 2.

118

### 119 ***In vitro* bactericidal assay**

120 3D4/31-PAMs ( $1 \times 10^6$  cells), *Escherichia coli* (*E. coli*) DH5 $\alpha$  ( $1 \times 10^7$  CFU, colony forming unit), and 5 % (v/v)  
121 porcine serum were mixed in a final volume of 1 mL of Hanks' balanced salt solution (HBSS, pH 7.4) and incubated  
122 at 37 °C for 1 h with shaking (180 rpm). After centrifugation at 12,000 RCF for 1 min, the supernatant (non-engulfed  
123 bacteria) was spread onto Luria-Bertani (LB; 244602, BD, Detroit, MI, USA) agar plates. The pelleted cells (with  
124 engulfed bacteria) were washed twice with HBSS, suspended in 1 mL of RPM1640 medium, and incubated for 0, 20,  
125 and 40 min at 37 °C with shaking (180 rpm). After each incubation period, the cells were lysed with dH<sub>2</sub>O for 5 min  
126 and spread on LB agar plates. The CFUs were counted after incubation for 12 h at 37 °C. Images of the LB agar plates  
127 were captured using iPhone X (Apple, Cupertino, CA, USA).

128

### 129 **Measurement of autophagic activity**

130 Cells were cultured with 1  $\mu$ g/mL acridine orange (A6014, Sigma-Aldrich) for 15 min, washed twice with PBS,  
131 harvested, washed with PBS, and analyzed by flow cytometry.

132

### 133 **Glucose uptake assay**

134 Cells were suspended in PBS containing 50  $\mu$ M 2-NBD-glucose (2-NBDG; 11046-10MG, Cayman Chemical,  
135 Ann Arbor, MI, USA) and 0.1 % (w/v) BSA, incubated for 30 min, washed with PBS, and analyzed by flow cytometry.

136

### 137 **Measurement of intracellular lipid droplet content**

138 Cells were cultured with 1  $\mu$ M BODIPY<sup>493/503</sup> (D3922, Invitrogen) for 30 min, washed twice with PBS, and  
139 subjected to fluorescence microscopy or flow cytometry. For flow cytometry, cells were harvested, washed with PBS,  
140 and analyzed.

141

### 142 **Visualization and quantification glycogen**

143 Glycogens were visualized using Best's carmine staining [19] with minor modifications. Cells were fixed for 15

144 min with 3.8 % (w/v) formaldehyde, washed with PBS, and stained with 0.625 % (w/v) Best's carmine solution (C1022;  
145 Sigma-Aldrich) for 30 min. Cells were then rinsed twice with dH<sub>2</sub>O containing 2 % (v/v) methanol and 4 % (v/v)  
146 ethanol, washed with ethanol for 1 min, and imaged. Glycogen content was quantified using the anthrone method [20]  
147 with minor modifications. Cells (1×10<sup>5</sup>) were lysed in 50 μL of 30 % (w/v) KOH for 20 min at 100 °C and 350 μL of  
148 43 % (v/v) ethanol was added. The cell lysate (50 μL) was reacted with 100 μL of 0.2 % (w/v) anthrone (319899,  
149 Sigma-Aldrich) at 100 °C for 20 min. The OD<sub>620</sub> of the lysate and glucose (G8270, Sigma-Aldrich) standards were  
150 measured using a FilterMaxF3 microplate reader.

151

### 152 **Fractionation of AFWE**

153 Serial fractionation of AFWE was performed using ethyl acetate, ethyl ether, ethanol, and isopropyl ether (extra-  
154 pure grade). The AFWE was shaken in a specific solvent system for 10 min and allowed to stand at 25 °C until the  
155 mixture formed two layers (1-2 h). The organic layer was then concentrated to 20 × in DMSO using a rotary evaporator.

156

### 157 **LC-MS of AFWE**

158 LC was carried out using an Acquity UPLC system (Waters, Milford, MA, USA) with an Acquity BEH C18 1.7  
159 μm column (2.1 × 100 mm). The LC processed the samples at 0.2 mL/min using water/methanol with 0.1 % (v/v)  
160 formic acid at 40 °C. MS was performed using the SYNAPT G2 platform (Waters). Molecules were identified using  
161 m/z CLOUD (<https://www.mzcloud.org>) and molecular structures were illustrated using ChemDraw Ultra Ver. 12.0.2  
162 (CambridgeSoft, Cambridge, MA, USA).

163

### 164 **Computational prediction of molecular docking**

165 The 3D structure of porcine-P2Y<sub>14</sub> (AF-F1S3N3-F1) was downloaded from the AlphaFold Protein Structure  
166 Database Ver. 2022-11-01 (<https://alphafold.ebi.ac.uk>). The canonical SMILES of the ligands (Limonin #179651 and  
167 UDPG #8629, PubChem release 2021.10.14) were retrieved from the PubChem Database  
168 (<https://pubchem.ncbi.nlm.nih.gov>). Molecular docking and visualization were performed using DiffDock-L [21]  
169 hosted at Neurosnap.ai (<https://neurosnap.ai>).

170

### 171 **Flow cytometry analysis**

172 Flow cytometry was performed using a Guava easyCyte Flow Cytometer (Merck Millipore) and Guava InCyte



173 software Ver. 2.6. An average of  $3 \times 10^3$  cells was measured for the single-channel assay and an average of  $5 \times 10^3$  cells  
174 was measured for the dual-channel assay. Flow cytometry plots and fluorescence intensities were obtained using the  
175 FlowJo Ver. 10.6.2 (TreeStar, Ashland, OR, USA).

176

### 177 **Imaging and processing**

178 Microscopy was performed using DMI8 fluorescence microscope (Leica, Wetzlar, Germany). LAS X software  
179 Ver. 2.0.0.14332 was used for the fluorescence images, and LAS software Ver. 4.7.1 for the bright-field images. To  
180 display representative images, contrast and brightness adjustments were processed using Photoshop 2024 (Adobe  
181 Systems, San Jose, CA, USA).

182

### 183 **Statistical analysis**

184 Statistical analyses were based on at least 3 independent biological experiments and were performed using  
185 GraphPad PRISM software Ver. 10.2.3 (GraphPad Software, San Diego, CA, USA). All data are shown as mean  $\pm$   
186 standard deviation. Analysis of variance (ANOVA) with Tukey's multiple comparison test or unpaired two-tailed  
187 Student's t-test was used for statistical analyses. Statistical significance was set at  $p < 0.05$ .

188

189

190

## **RESULTS**

### 191 ***A. flagelliformis* water extract suppresses proinflammatory features in 3D4/31-PAMs**

192 To determine the anti-inflammatory properties of *A. flagelliformis*, we developed AFWE and evaluated its  
193 bioactivity against ROS production, cytokine expression, and bactericidal activity in 3D4/31-PAMs. First, fresh *A.*  
194 *flagelliformis* was extracted using a water extraction method (Fig. 1A and 1B). The dry weight of AFWE was found  
195 to be 6 mg/mL, giving an extraction efficiency of 1.8% based on the solid content. To determine the cytotoxicity of  
196 AFWE on pulmonary alveoli, WST8 was performed on 3D4/31-PAM and A549-AEC. Although AFWE was not  
197 cytotoxic to 3D4/31-PAMs, A549-AECs viability was increased by 60  $\mu$ g/mL AFWE and decreased by 6  $\mu$ g/mL  
198 AFWE treatment (Fig. 1C). As the number of tissue-resident AMs decreases with the severity of lung infection [22,  
199 23], we tested the protective effect of AFWE on the proliferation of 3D4/31-PAMs. However, 60  $\mu$ g/mL AFWE did  
200 not upregulate the proliferation of PMA-stimulated 3D4/31-PAMs (PS-3D4/31-PAMs) (Fig. 1D).

201 AFWE (0.006-60  $\mu\text{g}/\text{mL}$ ) reduced the intracellular ROS levels in PS-3D4/31-PAMs (Fig. 1E). 60  $\mu\text{g}/\text{mL}$  AFWE  
202 showed no antioxidant effect on unstimulated 3D4/31-PAMs (Fig. 1F). This antioxidant effect of AFWE on PS-  
203 3D4/31-PAM is supported by the inhibition of NADPH oxidase 2 (NOX2) complex expression, a source of ROS, in  
204 inflamed AMs [24]. AFWE (60  $\mu\text{g}/\text{mL}$ ) suppressed the expression of NOX2 complex, including gp91<sup>PHOX</sup> (NOX2)  
205 (Fig. 1G), *neutrophil cytosolic factor 2 (NCF2)*, *NCF1*, *NCF4*, and *cytochrome b-245 a chain (CYBA)* in PS-3D4/31-  
206 PAMs (Fig. 1H). Overall, 60  $\mu\text{g}/\text{mL}$  AFWE lowered ROS production via the downregulation of NOX2 without toxicity  
207 in 3D4/31-PAM. Furthermore, AFWE treatment at concentrations lower than 60  $\mu\text{g}/\text{mL}$  was toxic in A549-AEC, so  
208 we established 60  $\mu\text{g}/\text{mL}$  as the optimal AFWE concentration for alveolar immunomodulation and conducted  
209 subsequent experiments.

210 Next, we confirmed that AFWE inhibited proinflammatory gene expression and bactericidal activity in 3D4/31-  
211 PAMs. AFWE decreased the levels of proinflammatory markers such as COX2 (Fig. 2A), *prostaglandin-endoperoxide*  
212 *synthase 2 (PTGS2)*, *TNF*, and *interleukin 1  $\beta$  (IL1B)* (Fig. 2B) in PS-3D4/31-PAMs while slightly reducing the  
213 expression of the anti-inflammatory marker *ARG1* and *resistin-like  $\beta$  (RETNLB)* (Fig. 2B). Bactericidal assays (Fig.  
214 2C) revealed that AFWE diminished the bactericidal activity against *E. coli* DH5 $\alpha$  in 3D4/31-PAMs (Fig. 2D and 2E).  
215 Moreover, AFWE reduced the *E. coli*-induced autophagy (Fig. 2F). These results indicate that AFWE downregulates  
216 proinflammatory features, including ROS production, proinflammatory gene expression, and bactericidal activity, in  
217 3D4/31-PAMs.

218

### 219 ***A. flagelliformis* water extract suppresses P2Y<sub>14</sub>-associated metabolism in 3D4/31-PAMs**

220 To confirm whether AFWE regulates P2Y<sub>14</sub>-associated metabolism in PAMs, glucose metabolism and P2Y<sub>14</sub>  
221 cascade were quantified. Glucose uptake was reduced (Fig. 3A), and the LD content was upregulated (Fig. 3B and 3C)  
222 by AFWE in the 3D4/31-PAMs. The increased glycogen content in 3D4/31-PAMs following PMA stimulation was  
223 prevented by AFWE treatment (Fig. 3D and 3E). Considering that lipid accumulation in polarized macrophages  
224 depends on fatty acid uptake [25], our results indicate that AFWE selectively blocks P2Y<sub>14</sub> (glycogen)-mediated  
225 inflammation. Glucose uptake, glycogenesis, and the pentose phosphate pathway (PPP) are essential for P2Y<sub>14</sub>-  
226 mediated proinflammatory responses. In particular, activation of the glycogenesis, characterized by intracellular  
227 glycogen accumulation, is required for the production of the P2Y<sub>14</sub> ligand UDPG [10] (Fig. 3F). qRT-PCR showed  
228 that AFWE suppressed the expression of genes related to glucose uptake (*SLC2A1*, *solute carrier family 2 member 1*),  
229 glycogenesis (*PGM1*, *phosphoglucomutase 1*; *PYGL*, *glycogen phosphorylase L*; *GAA*,  *$\alpha$ -glucosidase*), and PPP

230 (*G6PD*, *glucose-6-phosphate dehydrogenase*; *TKT*, *transketolase*) in the 3D4/31-PAMs (Fig. 3G and 3H). AFWE  
231 suppressed *P2RY14* and *STAT1* expression in the PS-3D4/31-PAMs (Fig. 3I), suggesting that AFWE suppresses  
232 metabolism related to P2Y<sub>14</sub> activation. These results suggest that AFWE suppresses P2Y<sub>14</sub>-associated  
233 proinflammatory features in PAMs

234

### 235 **Identification of potential P2Y<sub>14</sub> antagonistic compound in *A. flagelliformis* water extract**

236 Polarity-based fractionation and LC-MS were performed to identify anti-inflammatory compounds in AFWE.  
237 The obtained fractions were concentrated 20-fold before use, and the dry weight of AFWE-OL3 was 52 mg/mL (Fig.  
238 4A). AFWE-OL3 (52 µg/mL) reduced the levels of P2Y<sub>14</sub> and PYGL in the immunoblotting of 3D4/31-PAMs (Fig.  
239 4B). Genetic or chemical inhibition of PYGL can effectively inhibit P2Y<sub>14</sub>-mediated cytokine expression by reducing  
240 NADPH production [10]. The LC chromatogram of AFWE-OL3 showed a major peak at retention time (RT) 9.56  
241 (Fig. 4C). The mass spectrum of RT9.56 was analyzed using the m/z CLOUD Mass Spectral Database, and the most  
242 similar compound was identified as limonin, also known as obaculactone and evodin (Fig. 4D). Based on the peak  
243 area (39%) at RT 9.56, AFWE-OL3 is expected to contain 28.42 mg/mL limonin. Considering that AFWE-OL3 was  
244 20-fold enriched, it is estimated that limonin is present in AFWE at a concentration of 1.42 mg/mL. Limonin (Fig.  
245 4E), a limonoid polyphenol found in citrus, has been reported to protect against lipopolysaccharide (LPS)-induced  
246 acute lung injury [26]. Interestingly, in citrus fruits, the glucose unit of UDPG can be transferred to limonin by  
247 limonoid glucosyltransferase [27].

248 To assess the potential interaction between limonin and porcine-P2Y<sub>14</sub>, we performed computational molecular  
249 docking analysis. The structure of the porcine-P2Y<sub>14</sub> (Fig. 4F) used in this study exhibited a very high confidence for  
250 ARG253/LYS277/GLU278 (Fig. 4G), a key amino acid in the interaction between P2Y<sub>14</sub> and UDPG [28]. Our  
251 prediction showed that UDPG interacts with ARG253/LYS277/GLU278 in porcine-P2Y<sub>14</sub> (Fig. 4H). The prediction  
252 of limonin docking to porcine-P2Y<sub>14</sub> showed consistency in limonin poses (Fig. 4I). The prediction model with the  
253 highest score showed an interaction between limonin and ARG253/LYS277 (Fig. 4J). These results suggest the  
254 potential binding of limonin to the UDPG-binding site of porcine-P2Y<sub>14</sub>.

255

### 256 **Limonin suppresses UDPG-induced proinflammatory gene expression in 3D4/31-PAMs**

257 To confirm the anti-inflammatory effect of limonin on PAMs, we assessed the dose-response effect of limonin  
258 on viability and proinflammatory gene expression. Limonin treatment, at a final concentration of 30 µM, increased

259 the viability of 3D4/31-PAMs cultured with or without PMA (Fig. 5A). Dose-response screening of limonin using  
260 qRT-PCR showed that 30  $\mu$ M limonin suppressed the expression of *P2RY14*, *STAT1*, and *PTGS2*, but not *ARG1*, in  
261 PS-3D4/31-PAMs (Fig. 5B). Based on these results, we suggest that limonin at a final concentration of 30  $\mu$ M has the  
262 potential to suppress P2Y<sub>14</sub>-mediated inflammation in PAMs.

263 Next, to assess the effects of limonin on UDPG-induced inflammation, 3D4/31-PAMs were stimulated with  
264 combination of PMA with UDPG. Significantly increased expression levels of *retinoic acid receptor  $\beta$*  (*RARB*), *STAT1*,  
265 *PTGS2*, and arginase-1 (*ARG1*) were observed in 3D4/31-PAMs stimulated with 200  $\mu$ M UDPG. Limonin treatment  
266 suppressed the expression of *P2RY14*, *RARB*, *STAT1*, *PTGS2*, and *ARG1* in 3D4/31-PAMs stimulated with  
267 PMA/UDPG (200  $\mu$ M) (Fig. 5C). The PMA/UDPG-induced ROS production in 3D4/31-PAMs was reduced by  
268 limonin treatment (Fig. 5D). These results suggest that limonin has the potential to suppress UDPG/P2Y<sub>14</sub>-induced  
269 inflammation in PAMs.

270

271

272

## DISCUSSION

273 PRDC remain the most serious threat to pig health and productivity. This study sought to explore the association  
274 of P2Y<sub>14</sub> with porcine respiratory inflammation and to develop a new AID. AFWE inhibited ROS production by  
275 reducing the expression of NOX family members in PS-3D4/31-PAMs and suppressed glucose uptake and  
276 glycogenesis. We also demonstrated the potential of AFWE to inhibit P2Y<sub>14</sub>-mediated inflammation by reducing the  
277 expression of *P2RY14*, *STAT1*, *TNF*, *IL1B*, and *PTGS2*. Limonin reduced the UDPG-induced expression of *P2RY14*,  
278 *RARB*, *STAT1*, and *PTGS2* in 3D4/31-PAMs. These results suggest the involvement of P2Y<sub>14</sub> as a major regulator of  
279 inflammatory responses in PAMs and propose AFWE and limonin as AID candidates that can control this receptor.

280 Macrophages under inflammatory stimuli or after phagocytosis of bacteria increase cytokine and ROS production  
281 to recruit immune cells and eliminate pathogens [29]. AFWE inhibited NOX2 complex expression, ROS production,  
282 and bactericidal activity in 3D4/31-PAMs. These results are consistent with reports that NOX2 is a major source of  
283 ROS that kills phagocytic bacteria and that NOX2 deficiency impairs bactericidal activity [30]. AFWE inhibited the  
284 expression of proinflammatory genes *PTGS2*, *TNF*, and *IL1B* in 3D4/31-PAMs. TNF and IL1B induce macrophage  
285 activation and *PTGS2* expression. COX2 (encoded by *PTGS2*) is a major target for anti-inflammatory drug  
286 development, as it plays a central role in the regulation of inflammatory processes through the modulation of vascular  
287 permeability and tissue swelling [31]. Therefore, the inhibitory effect of AFWE and limonin on *PTGS2* expression

288 suggests their potential as anti-inflammatory drugs. ARG1 expression was increased by PMA in 3D4/31-PAMs and  
289 slightly reduced by AFWE. ARG1 is classically used as a marker of anti-inflammation; however, AMs have been  
290 reported to express both inflammatory and anti-inflammatory markers and express high levels of ARG1 under chronic  
291 infection [32, 33]. Therefore, we suggest that the increase in *ARG1* levels by PMA and UDPG is due to the metabolic  
292 features of AMs.

293 Glucose is essential for energy metabolism and P2Y<sub>14</sub>-mediated inflammation. AFWE slightly decreased the  
294 glucose uptake of 3D4/31-PAMs but increased the LD content and had no effect on viability and proliferation. Given  
295 the high dependence of AMs proliferation and development on fatty acid metabolism [34], we suggest that activation  
296 of fatty acid metabolism may have maintained energy metabolism. PMA treatment increased *SLC2A1* expression but  
297 decreased glucose uptake and did not increase P2Y<sub>14</sub> cascade gene expression. PMA/UDPG treatment increased *RARB*  
298 and *STAT1* expression, suggesting that P2Y<sub>14</sub>-mediated inflammation was activated. These results suggest that PMA  
299 is inadequate to induce P2Y<sub>14</sub> activation at the mRNA expression level, and that PMA/UDPG combination treatment  
300 is suitable for P2Y<sub>14</sub> activation in 3D4/31-PAM.

301 Increased P2Y<sub>14</sub> activity is closely related to the exacerbation of various diseases including asthma [35],  
302 coronavirus disease 2019 [36], gouty arthritis [37], and intestinal inflammation [38], suggesting a variety of  
303 therapeutic uses for P2Y<sub>14</sub> antagonists. In porcine, P2Y<sub>14</sub> has been reported as a therapeutic target for heart disease  
304 and diabetes [11, 18], and we demonstrated its role in porcine alveolar immunity. We observed increased glycogenesis,  
305 a characteristic feature of P2Y<sub>14</sub>-mediated inflammation, in PS-3D4/31-PAMs. These results suggest an increased  
306 glucose requirement by macrophages in inflammatory responses, and are consistent with LPS-induced increased  
307 glucose consumption and hypoglycemia [39]. Additionally, porcine skeletal muscle growth rate is associated with the  
308 expression of glycogenesis-related genes (*PGMI*, *phosphoglucomutase 1*; *UGP2*, *UDPG pyrophosphorylase 2*) [40].  
309 These findings make it interesting to study the effects of P2Y<sub>14</sub> and UDPG levels on porcine productivity.

310 The selection of extraction solvents considers various factors such as extraction efficiency, environmental hazards,  
311 and residual toxicity. In line with the global trend toward eco-friendly industries, the importance of water extraction  
312 technology is increasing [41]. Succulent *Opuntia* species, known to have potential as livestock feed [13], have been  
313 reported to lack antioxidant and antibacterial effects in aqueous extracts [42]. This is attributed to the low solubility  
314 of major bioactive compounds such as polyphenols in water [43]. Using LC-MS, we identified limonin as a potential  
315 bioactive compound in AFWE. Limonin can be extracted from *Citrus grandis* (pomelo) via water and resin absorption  
316 [44]. Additionally, limonin is abundant in the peel of *Citrus aurantifolia* (lime), which is often discarded as waste and

317 can be extracted using the low-toxicity solvent, ethanol [45]. In this study, the limonin content of AFWE estimated by  
318 LC-MS was 23.69% (w/v), 1.42 mg/mL. A 14.21  $\mu\text{g/mL}$  of limonin content was expected with 60  $\mu\text{g/mL}$  AFWE  
319 treatment, which was similar to the optimal anti-inflammatory activity concentration of 30  $\mu\text{M}$  (14.12  $\mu\text{g/mL}$ ) of  
320 limonin. This suggests that limonin confers anti-inflammatory activity to AFWE. Overall, these findings suggest that  
321 AFWE and limonin are promising AID candidates for the eco-friendly livestock industry.

322 Limonin has been noted for its various pharmacological activities but has limited clinical potential due to unclear  
323 mechanisms of action [46]. In this study, we confirmed that AFWE and limonin reduced PMA-induced expression of  
324 *PTGS2*, *STAT1*, and *P2RY14* in 3D4/31-PAMs. Our molecular docking prediction also indicated that limonin has a  
325 higher binding score to porcine-P2Y<sub>14</sub> than to UDPG. These results suggest that the potential mechanism of action  
326 (MOA) of AFWE and limonin involves binding to and inhibiting the activity of porcine-P2Y<sub>14</sub>. Further research is  
327 required to clarify this MOA, including confirmation of the nuclear localization of STAT1/RAR $\beta$ , which is  
328 characteristic of P2Y<sub>14</sub> activation [10]. Our molecular docking analysis used the predicted porcine-P2Y<sub>14</sub> structure  
329 due to the limited number of studies on porcine-P2Y<sub>14</sub>. Although UDPG binding to P2Y<sub>14</sub> induces structural changes  
330 [28], mechanical binding studies of limonin to porcine-P2Y<sub>14</sub> have not been conducted. Nevertheless, the reduction in  
331 the UDPG-induced expression of *RARB*, *STAT1*, and *PTGS2* in 3D4/31-PAMs by limonin suggests the potential of  
332 limonin to inhibit P2Y<sub>14</sub>-mediated inflammation.

333 In summary, AFWE exerted anti-inflammatory effects in 3D4/31-PAMs, inhibiting ROS production and  
334 *NOX2/PTGS2/TNFA* expression reported in PRDC. Limonin, a compound identified from AFWE, inhibited the  
335 UDPG-induced expression of P2Y<sub>14</sub> cascade genes and *PTGS2* in 3D4/31-PAMs. Overall, our results suggest that  
336 P2Y<sub>14</sub> is a target for the control of PRDC and provides new insights into the inflammatory response of PAMs.  
337 Furthermore, we propose AFWE and limonin as candidate AIDs for porcine.

338  
339  
340

## REFERENCES

- 342 1. Calderon Diaz JA, Fitzgerald RM, Shalloo L, Rodrigues da Costa M, Niemi J, Leonard FC, et al. Financial  
 343 Analysis of Herd Status and Vaccination Practices for Porcine Reproductive and Respiratory Syndrome Virus,  
 344 Swine Influenza Virus, and Mycoplasma hyopneumoniae in Farrow-to-Finish Pig Farms Using a Bio-Economic  
 345 Simulation Model. *Front Vet Sci.* 2020;7:556674. <https://doi.org/10.3389/fvets.2020.556674>.
- 346 2. Hansen MS, Pors SE, Jensen HE, Bille-Hansen V, Bisgaard M, Flachs EM, Nielsen OL. An investigation of the  
 347 pathology and pathogens associated with porcine respiratory disease complex in Denmark. *J Comp Pathol.*  
 348 2010;143(2-3):120-31. <https://doi.org/10.1016/j.jcpa.2010.01.012>.
- 349 3. Sanchez-Carvajal JM, Rodriguez-Gomez IM, Ruedas-Torres I, Larenas-Munoz F, Diaz I, Revilla C, et al.  
 350 Activation of pro- and anti-inflammatory responses in lung tissue injury during the acute phase of PRRSV-1  
 351 infection with the virulent strain Lena. *Vet Microbiol.* 2020;246:108744.  
 352 <https://doi.org/10.1016/j.vetmic.2020.108744>.
- 353 4. Schoos A, Devreese M, Maes DG. Use of non-steroidal anti-inflammatory drugs in porcine health management.  
 354 *Vet Rec.* 2019;185(6):172. <https://doi.org/10.1136/vr.105170>.
- 355 5. Chang HW, Jeng CR, Lin TL, Liu JJ, Chiou MT, Tsai YC, et al. Immunopathological effects of porcine circovirus  
 356 type 2 (PCV2) on swine alveolar macrophages by in vitro inoculation. *Vet Immunol Immunopathol.* 2006;110(3-  
 357 4):207-19. <https://doi.org/10.1016/j.vetimm.2005.09.016>.
- 358 6. Su ZJ, Yang J, Luo WJ, Wei YY, Shuai XH, Hu TJ. Inhibitory effect of Sophora subprostrate polysaccharide on  
 359 mitochondria oxidative stress induced by PCV-2 infection in RAW264.7 cells. *Int J Biol Macromol.*  
 360 2017;95:608-17. <https://doi.org/10.1016/j.ijbiomac.2016.11.101>.
- 361 7. Zhai N, Liu K, Li H, Liu Z, Wang H, Korolchuk VI, et al. PCV2 replication promoted by oxidative stress is  
 362 dependent on the regulation of autophagy on apoptosis. *Vet Res.* 2019;50(1):19. <https://doi.org/10.1186/s13567-019-0637-z>.
- 364 8. Liu D, Lin J, Su J, Chen X, Jiang P, Huang K. Glutamine Deficiency Promotes PCV2 Infection through Induction  
 365 of Autophagy via Activation of ROS-Mediated JAK2/STAT3 Signaling Pathway. *J Agric Food Chem.*  
 366 2018;66(44):11757-66. <https://doi.org/10.1021/acs.jafc.8b04704>.
- 367 9. Yang J, Cao MX, Hu WY, Wei YY, Hu TJ. Sophora subprostrate polysaccharide suppress the inflammatory  
 368 reaction of RAW264.7 cells infected with PCV2 via regulation NF- $\kappa$ B/MAPKs/c-Jun signal pathway and histone  
 369 acetylation modification. *Int J Biol Macromol.* 2020;159:957-65. <https://doi.org/10.1016/j.ijbiomac.2020.05.128>.
- 370 10. Ma J, Wei K, Liu J, Tang K, Zhang H, Zhu L, et al. Glycogen metabolism regulates macrophage-mediated acute  
 371 inflammatory responses. *Nat Commun.* 2020;11(1):1769. <https://doi.org/10.1038/s41467-020-15636-8>.
- 372 11. Abbas ZSB, Latif ML, Dovlatova N, Fox SC, Heptinstall S, Dunn WR, Ralevic V. UDP-sugars activate P2Y(14)  
 373 receptors to mediate vasoconstriction of the porcine coronary artery. *Vascul Pharmacol.* 2018;103-105:36-46.  
 374 <https://doi.org/10.1016/j.vph.2017.12.063>.

- 375 12. Wang J, Lyu W, Zhang W, Chen Y, Luo F, Wang Y, et al. Discovery of natural products capable of inducing  
376 porcine host defense peptide gene expression using cell-based high throughput screening. *J Anim Sci Biotechnol.*  
377 2021;12(1):14. <https://doi.org/10.1186/s40104-020-00536-0>.
- 378 13. Pastorelli G, Serra V, Vannuccini C, Attard E. *Opuntia* spp. as Alternative Fodder for Sustainable Livestock  
379 Production. *Animals (Basel).* 2022;12(13). <https://doi.org/10.3390/ani12131597>.
- 380 14. Xu Z, Liu Y, Peng P, Liu Y, Huang M, Ma Y, et al. Aloe extract inhibits porcine epidemic diarrhea virus in vitro  
381 and in vivo. *Vet Microbiol.* 2020;249:108849. <https://doi.org/10.1016/j.vetmic.2020.108849>.
- 382 15. Kim H, Jeon EH, Park BC, Kim SJ. *Dudleya brittonii* extract promotes survival rate and M2-like metabolic  
383 change in porcine 3D4/31 alveolar macrophages. *Asian-Australas J Anim Sci.* 2019;32(11):1789-800.  
384 <https://doi.org/10.5713/ajas.19.0251>.
- 385 16. Lozoya X. Mexican medicinal plants used for treatment of cardiovascular diseases. *Am J Chin Med.*  
386 1980;8(01n02):86-95. <https://doi.org/10.1142/s0192415x80000074>.
- 387 17. Andrade-Cetto A, Heinrich M. Mexican plants with hypoglycaemic effect used in the treatment of diabetes. *J*  
388 *Ethnopharmacol.* 2005;99(3):325-48. <https://doi.org/10.1016/j.jep.2005.04.019>.
- 389 18. Alsaqati M, Latif ML, Chan SL, Ralevic V. Novel vasocontractile role of the P2Y(1)(4) receptor: characterization  
390 of its signalling in porcine isolated pancreatic arteries. *Br J Pharmacol.* 2014;171(3):701-13.  
391 <https://doi.org/10.1111/bph.12473>.
- 392 19. Horobin R, Murgatroyd L. The staining of glycogen with Best's Carmine and similar hydrogen bonding dyes. A  
393 mechanistic study. *Histochem J.* 1971;3:1-9. <https://doi.org/10.1007/BF01686501>.
- 394 20. Carroll NV, Longley RW, Roe JH. The determination of glycogen in liver and muscle by use of anthrone reagent.  
395 *J Biol Chem.* 1956;220(2):583-93. [https://doi.org/10.1016/S0021-9258\(18\)65284-6](https://doi.org/10.1016/S0021-9258(18)65284-6).
- 396 21. Corso G, Stärk H, Jing B, Barzilay R, Jaakkola T. Diffdock: Diffusion steps, twists, and turns for molecular  
397 docking. *arXiv.* 2022. <https://doi.org/10.48550/arXiv.2210.01776>.
- 398 22. Chen ST, Park MD, Del Valle DM, Buckup M, Tabachnikova A, Thompson RC, et al. A shift in lung macrophage  
399 composition is associated with COVID-19 severity and recovery. *Science Translational Medicine.* 2022;14(662).  
400 <https://doi.org/ARTN eabn5168>
- 401 10.1126/scitranslmed.abn5168.
- 402 23. de Oliveira VLS, Pollenus E, Berghmans N, Queiroz CM, Blanter M, Mattos MS, et al. Absence of CCR2  
403 Promotes Proliferation of Alveolar Macrophages That Control Lung Inflammation in Acute Respiratory Distress  
404 Syndrome in Mice. *Int J Mol Sci.* 2022;23(21). <https://doi.org/ARTN 1292010.3390/ijms232112920>.



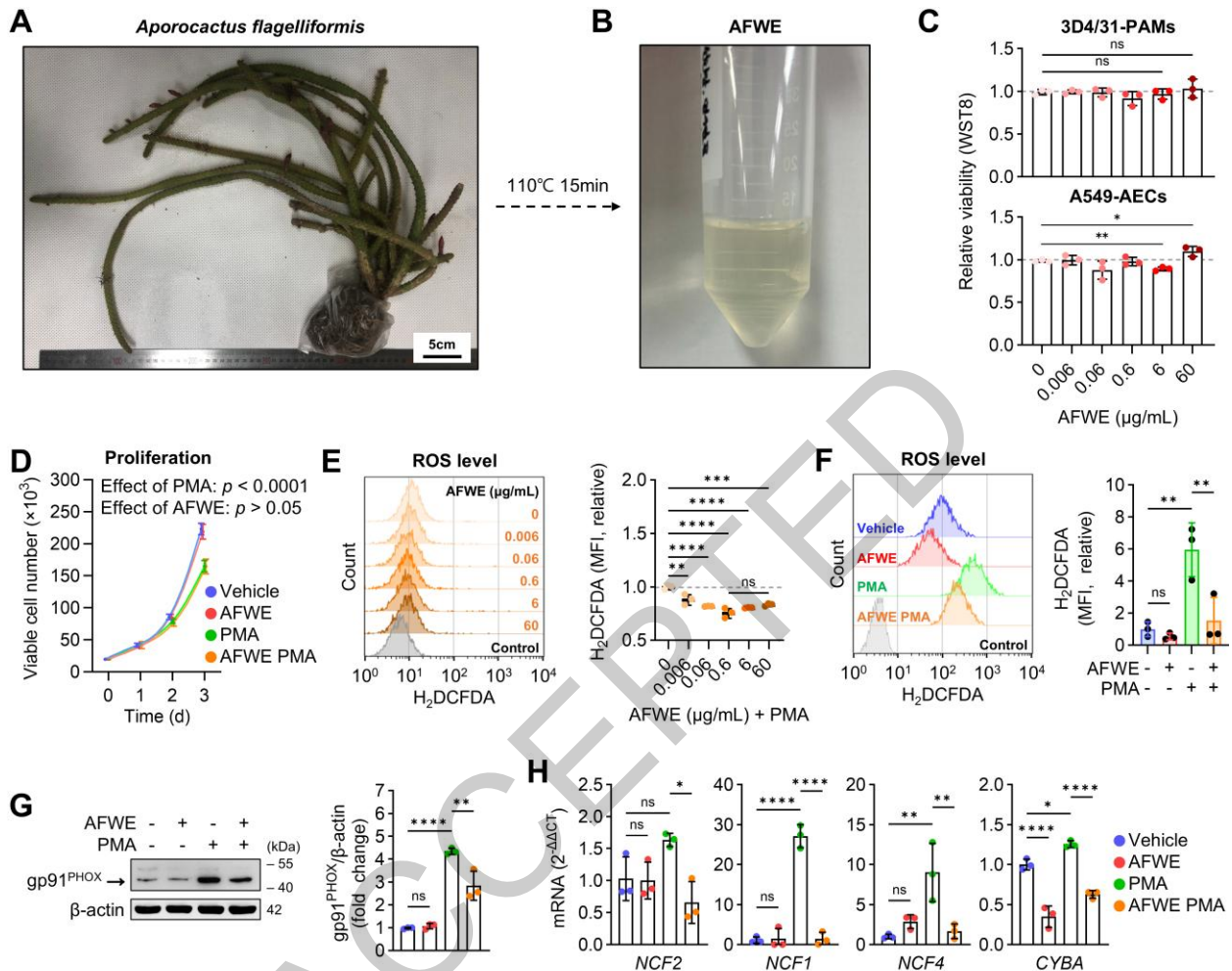
- 405 24. Caceres L, Paz ML, Garces M, Calabro V, Magnani ND, Martinefski M, et al. NADPH oxidase and mitochondria  
406 are relevant sources of superoxide anion in the oxinflammatory response of macrophages exposed to airborne  
407 particulate matter. *Ecotoxicol Environ Saf.* 2020;205:111186. <https://doi.org/10.1016/j.ecoenv.2020.111186>.
- 408 25. Knight M, Braverman J, Asfaha K, Gronert K, Stanley S. Lipid droplet formation in *Mycobacterium tuberculosis*  
409 infected macrophages requires IFN-gamma/HIF-1alpha signaling and supports host defense. *PLoS Pathog.*  
410 2018;14(1):e1006874. <https://doi.org/10.1371/journal.ppat.1006874>.
- 411 26. Liang H, Liu G, Fan Q, Nie Z, Xie S, Zhang R. Limonin, a novel AMPK activator, protects against LPS-induced  
412 acute lung injury. *Int Immunopharmacol.* 2023;122:110678. <https://doi.org/10.1016/j.intimp.2023.110678>.
- 413 27. Karim MR, Hashinaga F. Isolation and characterization of limonoid glucosyltransferase from pummelo albedo  
414 tissue. *Food Chem.* 2002;76(4):431-6. [https://doi.org/10.1016/S0308-8146\(01\)00300-4](https://doi.org/10.1016/S0308-8146(01)00300-4).
- 415 28. Zhao L, Wei F, He X, Dai A, Yang D, Jiang H, et al. Identification of a carbohydrate recognition motif of  
416 purinergic receptors. *Elife.* 2023;12. <https://doi.org/10.7554/eLife.85449>.
- 417 29. Nonnenmacher Y, Hiller K. Biochemistry of proinflammatory macrophage activation. *Cell Mol Life Sci.*  
418 2018;75(12):2093-109. <https://doi.org/10.1007/s00018-018-2784-1>.
- 419 30. Márquez JDR, Li TYN, McCluggage ARR, Tan JMJ, Muise A, Higgins DE, Brumell JH. Cutting Edge: NOX2  
420 NADPH Oxidase Controls Infection by an Intracellular Bacterial Pathogen through Limiting the Type 1 IFN  
421 Response. *J Immunol.* 2021;206(2):323-8. <https://doi.org/10.4049/jimmunol.2000694>.
- 422 31. Ahmadi M, Bekeschus S, Weltmann KD, von Woedtke T, Wende K. Non-steroidal anti-inflammatory drugs:  
423 recent advances in the use of synthetic COX-2 inhibitors. *RSC Med Chem.* 2022;13(5):471-96.  
424 <https://doi.org/10.1039/d1md00280e>.
- 425 32. Mitsi E, Kamng'ona R, Rylance J, Solorzano C, Jesus Reine J, Mwandumba HC, et al. Human alveolar  
426 macrophages predominately express combined classical M1 and M2 surface markers in steady state. *Respir Res.*  
427 2018;19(1):66. <https://doi.org/10.1186/s12931-018-0777-0>.
- 428 33. Hansakon A, Ngamphiw C, Tongsimma S, Angkasekwinai P. Arginase 1 Expression by Macrophages Promotes  
429 Proliferation and Invasion into Brain Microvascular Endothelial Cells. *J Immunol.* 2023;210(4):408-19.  
430 <https://doi.org/10.4049/jimmunol.2200592>.
- 431 34. Sinclair C, Bommakanti G, Gardinassi L, Loebbermann J, Johnson MJ, Hakimpour P, et al. mTOR regulates  
432 metabolic adaptation of APCs in the lung and controls the outcome of allergic inflammation. *Science.*  
433 2017;357(6355):1014-21. <https://doi.org/10.1126/science.aaj2155>.
- 434 35. Karcz TP, Whitehead GS, Nakano K, Nakano H, Grimm SA, Williams JG, et al. UDP-glucose and P2Y14  
435 receptor amplify allergen-induced airway eosinophilia. *J Clin Invest.* 2021;131(7).  
436 <https://doi.org/10.1172/JCI140709>.

- 437 36. Petiz LL, Glaser T, Scharfstein J, Ratajczak MZ, Ulrich H. P2Y14 Receptor as a Target for Neutrophilia  
438 Attenuation in Severe COVID-19 Cases: From Hematopoietic Stem Cell Recruitment and Chemotaxis to  
439 Thrombo-inflammation. *Stem Cell Rev Rep*. 2021;17(1):241-52. <https://doi.org/10.1007/s12015-021-10129-7>.
- 440 37. Li HW, Jiang WJ, Ye SM, Zhou MZ, Liu CX, Yang XP, et al. P2Y14 receptor has a critical role in acute gouty  
441 arthritis by regulating pyroptosis of macrophages. *Cell Death Dis*. 2020;11(5). <https://doi.org/10.1038/s41419-020-2609-7>.  
442
- 443 38. Liu L, Ito T, Li B, Tani H, Okuzaki D, Motooka D, et al. The UDP-glucose/P2Y14 receptor axis promotes  
444 eosinophil-dependent large intestinal inflammation. *Int Immunol*. 2024;36(4):155-66.  
445 <https://doi.org/10.1093/intimm/dxad050>.
- 446 39. Kvidera SK, Horst EA, Mayorga EJ, Sanz-Fernandez MV, Abuajamieh M, Baumgard LH. Estimating glucose  
447 requirements of an activated immune system in growing pigs. *J Anim Sci*. 2017;95(11):5020-9.  
448 <https://doi.org/10.2527/jas2017.1830>.
- 449 40. Li MZ, Li XW, Zhu L, Teng XK, Xiao HS, Shuai SR, et al. Differential expression analysis and regulatory  
450 network reconstruction for genes associated with muscle growth and adipose deposition in obese and lean pigs.  
451 *Prog Nat Sci-Mater*. 2008;18(4):387-99. <https://doi.org/10.1016/j.pnsc.2007.10.011>.
- 452 41. Gallina L, Cravotto C, Capaldi G, Grillo G, Cravotto G. Plant Extraction in Water: Towards Highly Efficient  
453 Industrial Applications. *Processes*. 2022;10(11). <https://doi.org/10.3390/pr10112233>.
- 454 42. Cho JY, Park SC, Kim TW, Kim KS, Song JC, Kim SK, et al. Radical scavenging and anti-inflammatory activity  
455 of extracts from *Opuntia humifusa* Raf. *J Pharm Pharmacol*. 2006;58(1):113-9.  
456 <https://doi.org/10.1211/jpp.58.1.0014>.
- 457 43. Minode M, Kadota K, Kawabata D, Yoshida M, Shirakawa Y. Enhancement in dissolution behavior and  
458 antioxidant capacity of quercetin with amino acids following radical formation via mechanochemical technique.  
459 *Adv Powder Technol*. 2022;33(5). <https://doi.org/10.1016/j.apt.2022.103582>.
- 460 44. Yang YF, Zhang LZ, Du XP, Zhang SF, Li LJ, Jiang ZD, et al. Recovery and purification of limonin from  
461 pummelo [*Citrus grandis*] peel using water extraction, ammonium sulfate precipitation and resin adsorption. *J  
462 Chromatogr B Analyt Technol Biomed Life Sci*. 2017;1060:150-7.  
463 <https://doi.org/10.1016/j.jchromb.2017.05.036>.
- 464 45. Phucharoenrak P, Muangnoi C, Trachootham D. A Green Extraction Method to Achieve the Highest Yield of  
465 Limonin and Hesperidin from Lime Peel Powder (*Citrus aurantifolia*). *Molecules*. 2022;27(3).  
466 <https://doi.org/10.3390/molecules27030820>.
- 467 46. Fan S, Zhang C, Luo T, Wang J, Tang Y, Chen Z, Yu L. Limonin: A Review of Its Pharmacology, Toxicity, and  
468 Pharmacokinetics. *Molecules*. 2019;24(20). <https://doi.org/10.3390/molecules24203679>.

469

470 **Figure Legends**

471



472

473 **Fig. 1. Development of AFWE and its antioxidant effects on 3D4/31-PAMs.** (A) Representative image of the *A.*

474 *flagelliformis* used in this study. (B) Representative image of *A. flagelliformis* water extract (AFWE). (C) Viability of

475 the 3D4/31-PAMs and A549-AECs treated with AFWE for 48 h (n = 3). *p* by two-tailed Student's T-test. (D)

476 Proliferation of 3D4/31-PAMs treated with AFWE and PMA (n = 3). *p* by three-way ANOVA. (E-F) Intracellular

477 ROS levels in 3D4/31-PAMs treated with AFWE for 24 h and PMA for 2 h (n = 3). (E) Dose-response screening of

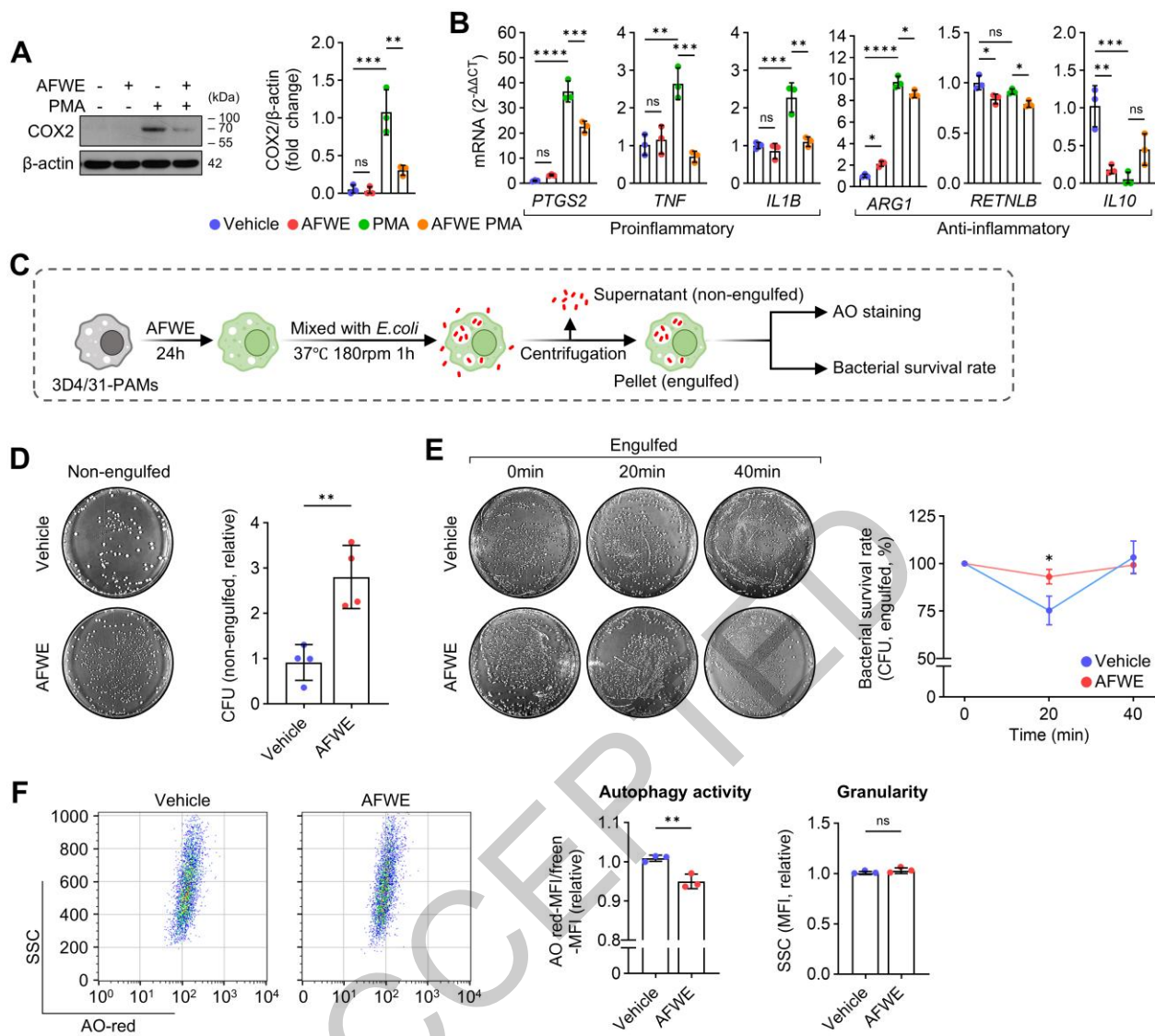
478 AFWE with PMA. (F) Intracellular ROS levels in the presence or absence of PMA. (G) Immunoblotting of gp91<sup>PHOX</sup>

479 in 3D4/31-PAMs treated with AFWE for 24 h and PMA for 12 h (n = 3). (H) Expression of NOX-related genes in

480 3D4/31-PAMs treated with AFWE for 24 h and PMA for 4 h (n = 3). *p* by one-way ANOVA. <sup>ns</sup>*p* > 0.05, \**p* < 0.05,

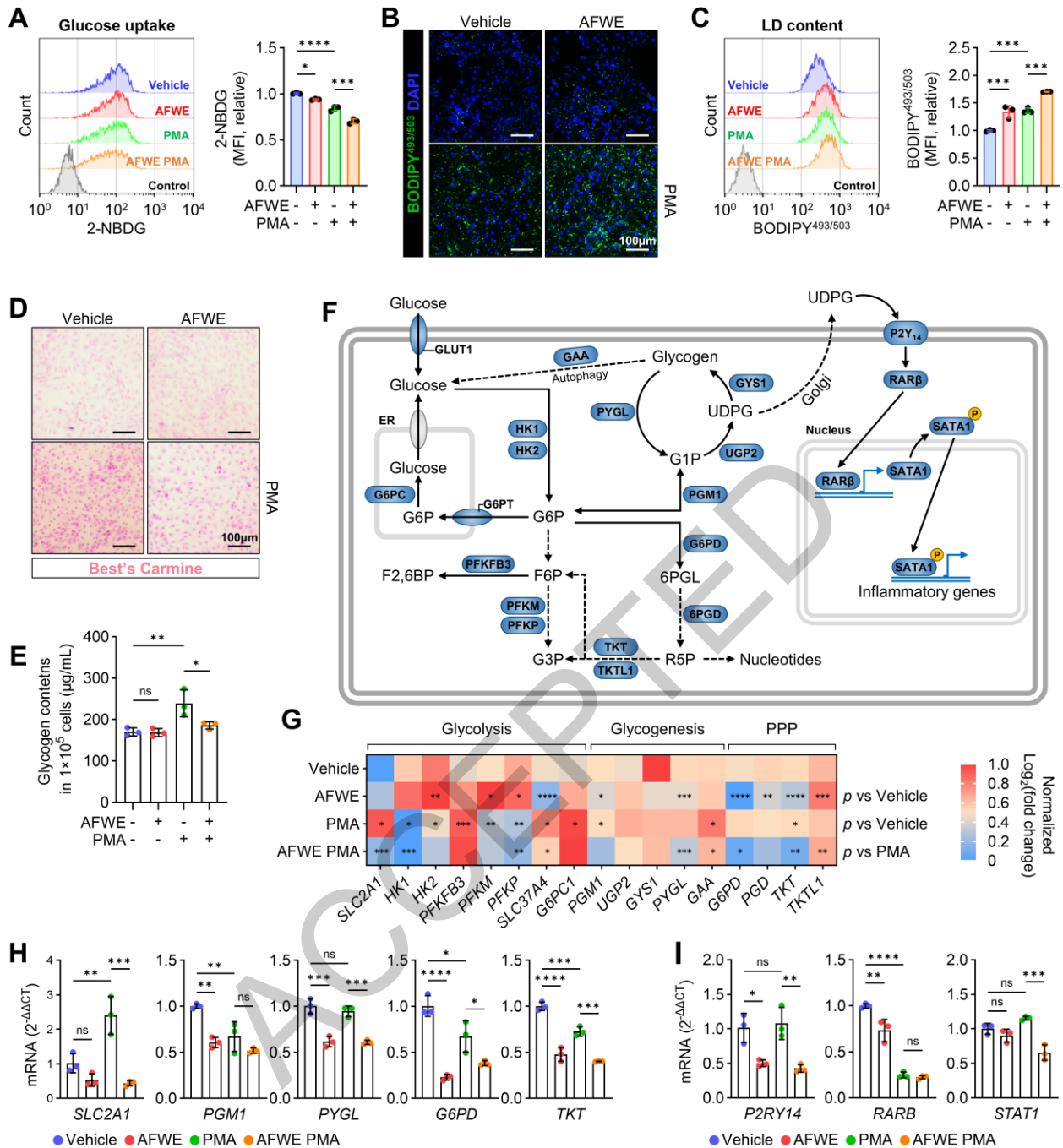
481 \*\**p* < 0.01, \*\*\**p* < 0.001, and \*\*\*\**p* < 0.0001.

482



483  
484 **Fig. 2. AFWE suppresses proinflammatory gene expression and bactericidal activity in 3D4/31-PAMs.** (A)  
485 Immunoblotting of COX2 in 3D4/31-PAMs treated with AFWE for 24 h and PMA for 12 h. (B) Expression of  
486 inflammation-related genes in 3D4/31-PAMs treated with AFWE for 24 h and PMA for 4 h. *p* by one-way ANOVA.  
487 (C-F) *In vitro* bactericidal assay of 3D4/31-PAMs treated with AFWE for 24 h. (C) Graphical scheme of the *in vitro*  
488 bactericidal assay. (D) Representative images and levels of non-engulfed bacteria (*n* = 4). *p* by unpaired two-tailed  
489 Student's *t*-test. (E) Representative images and bacterial survival rates (normalized to each time point at 0 h) (*n* = 3).  
490 *p* by two-way ANOVA. (F) Autophagic activity was quantified using flow cytometry with acridine orange (AO).  
491 Intracellular granularity (SSC, side scatter) is shown (*n* = 3). *p* by unpaired two-tailed Student's *t*-test. <sup>ns</sup>*p* > 0.05, \**p*  
492 < 0.05, \*\**p* < 0.01, \*\*\**p* < 0.001, and \*\*\*\**p* < 0.0001.

493  
494



495

496 **Fig. 3. AFWE suppresses P2Y<sub>14</sub>- associated metabolism in 3D4/31-PAMs.** (A) The glucose uptake rate in 3D4/31-

497 PAMs treated with AFWE for 24 h and PMA for 2 h (n = 3). (B-D) 3D4/31-PAMs treated with AFWE for 24 h and

498 PMA for 24 h (n = 3). (B-C) Fluorescence microscopy (B) and flow cytometry (C) of LD content in 3D4/31-PAMs.

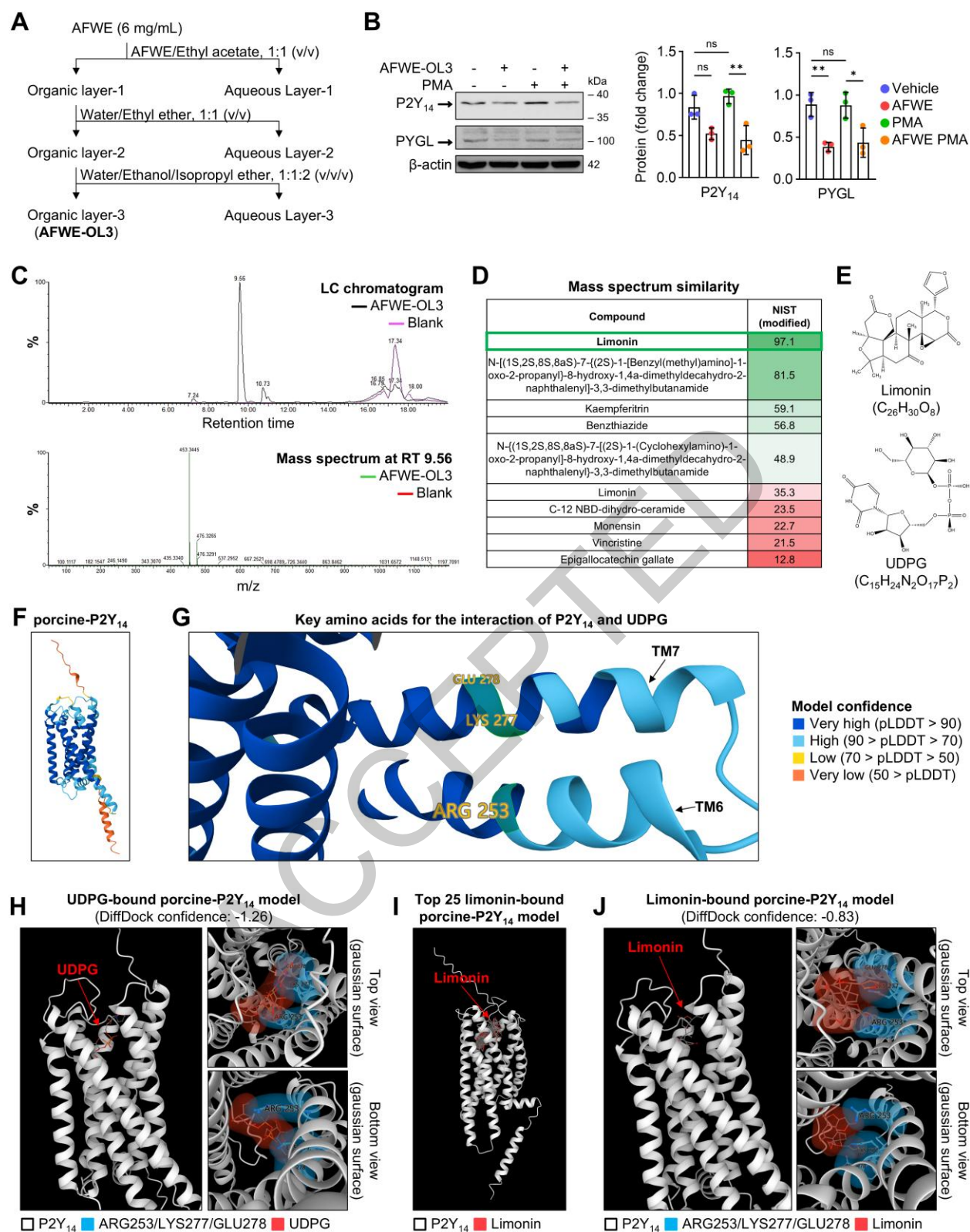
499 (D) Best's Carmine glycogen staining. (E) Quantification of glycogen content by using anthrone. (G-I) Expression of

500 genes related to P2Y<sub>14</sub> activation in 3D4/31-PAMs treated with AFWE for 24 h and PMA for 4 h (n = 3). (G)

501 Normalized Log<sub>2</sub>(fold change) of the genes. (H-I) Representative gene expression. *p* by one-way ANOVA. ns *p* > 0.05,

502 \**p* < 0.05, \*\**p* < 0.01, \*\*\**p* < 0.001, and \*\*\*\**p* < 0.0001.





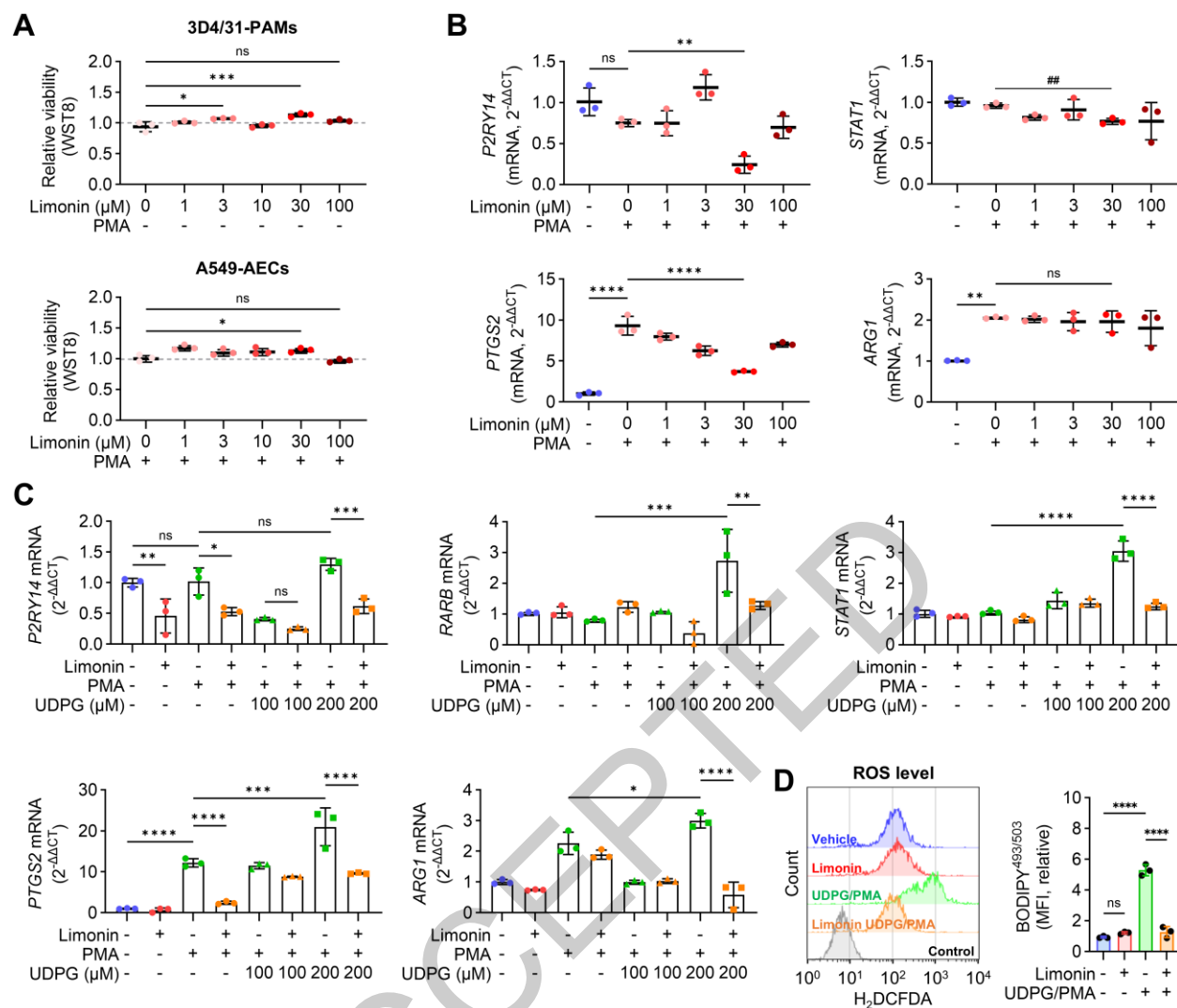
503

504

505 **Fig. 4. Identification of anti-inflammatory substances in AFWE.** (A) Experimental scheme for fractionation of506 AFWE. (B) Immunoblotting of P2Y<sub>14</sub> and PYGL in 3D4/31-PAMs treated with 73 μg/mL AFWE-OL3 for 24 h and

507 with PMA for 12 h (n = 3). *p* by one-way ANOVA. <sup>ns</sup>*p* > 0.05, \**p* < 0.05, and \*\**p* < 0.01. (C) LC-MS spectrum of the  
508 AFWE-OL3. (D) Mass spectrum similarity based on modified NIST (National Institute of Standards and Technology)  
509 score. (E) Structure of limonin and UDPG. (F-G) Protein structural model of porcine-P2Y<sub>14</sub> (F) and the positions of  
510 ARG253, LYS277, and GLU278 (G) in porcine-P2Y<sub>14</sub> (TM, transmembrane). Colored by model confidence (pLDDT,  
511 per-residue confidence score). (H) Predicted model for the UDPG-bound porcine-P2Y<sub>14</sub>. (I-J) Prediction model for  
512 limonin-bound porcine-P2Y<sub>14</sub>. (I) Top 25 modes. (J) Representative model with the highest DiffDock confidence level.  
513  
514

ACCEPTED



515

516

517 **Fig. 5. Limonin suppresses P2Y<sub>14</sub>-associated proinflammatory features in 3D4/31-PAMs.** (A) Viability of

518 3D4/31-PAMs and A549-AECs treated with limonin for 24 h and PMA for 24 h (n = 3). (B) Inflammatory gene

519 expression in 3D4/31-PAMs treated with limonin for 24 h and PMA for 4 h (n = 3). ##*p* < 0.01 by unpaired two-tailed

520 Student's t-test. (C) Expression of genes related to P2Y<sub>14</sub> activation in 3D4/31-PAMs treated with limonin for 24 h

521 and PMA/UDPG for 4 h. (D) Intracellular ROS levels in 3D4/31-PAMs treated with AFWE for 24 h and PMA/UDPG

522 for 2 h (n = 3). *p* by one-way ANOVA. *p* by one-way ANOVA, <sup>ns</sup>*p* > 0.05, \**p* < 0.05, \*\**p* < 0.01, \*\*\**p* < 0.001, and

523 \*\*\*\**p* < 0.0001.

524



525

## Tables and Figures

526 **Table 1. Antibodies used in this study for immunoblotting**

<b>Antibody (dilution)</b>	<b>Catalog No.</b>	<b>Manufacturers</b>
Anti- $\beta$ -actin antibody (1:10000)	A5441	Sigma-Aldrich
Anti-gp91 <sup>PHOX</sup> antibody (1:1000)	sc-20782	Santa Cruz Biotechnology
Anti-COX2 antibody (1:500)	sc-19999	Santa Cruz Biotechnology
Anti-P2Y <sub>14</sub> antibody (1:500)	ab136264	Abcam
Anti-PYGL antibody (1:500)	ab190243	Abcam
Anti-mouse IgG, HRP-linked antibody (1:5000)	#7076	Cell signaling
Anti-rabbit IgG, HRP-linked antibody (1:5000)	#7074S	Cell signaling

527

ACCEPTED

**Table 2. Primers sequences used in this study for qRT-PCR**

Gene symbol (accession)	Sense (5' to 3')	Antisense (5' to 3')
<i>RPS29</i> (NM_001001633.2)	CGGAAATACGGCTCAATATG	GCCAATATCCTTCGCGTACTG
<i>NCF2</i> (NM_001123142.1)	GTGAATGAAGAGTGGCCGGA	CAAATCTGTGGTTGCGCGTT
<i>NCF1</i> (NM_001113220.1)	GCGGGGAATCCATTGCAAAA	CTGCAACGGTGCAAGATGAG
<i>NCF4</i> (XM_013997542.2)	GTGCAGCTCATGGTGAGACA	TGGGTGATATGCAGCTTCCAG
<i>CYBA</i> (NM_214267.1)	GGAGCGCTGCGAACAAAAGT	CAGGAAGGCCCGGATGTAGT
<i>PTGS2</i> (NM_214321.1)	AATGGACGATGAACGGCTG	TGAAGTGGTAGCCACTCAGG
<i>TNF</i> (NM_214022.1)	CGTTGTAGCCAATGTCA	TAGGAGACGGCGATGC
<i>IL1B</i> (NM_214055.1)	TGCAAGGAGATGATAGCAACAAC	TCTCCATGTCCCTCTTTGGGT
<i>ARG1</i> (NM_214048.2)	GTGGACCCTGCAGAACACTA	ACCTTGCCAATTCCCAGCTT
<i>RETLNB</i> (NM_001103210.1)	AATCGCAAGGGGTTCTCAGT	TTGGAGCAGAGGGATTGAGC
<i>IL10</i> (NM_214041.1)	CGGCGCTGTCATCAATTCT	GGCTTTGTAGACACCCCTCTC
<i>SLC2A1</i> (XM_021096908.1)	CTGCTCATCAACCGCAATGA	GGCTCTCCTCCTTCATCTCC
<i>HK1</i> (NM_001243184.1)	GCACGATGTGGTGACCTTAC	CCAGTCCCTACGATGAGTCC
<i>HK2</i> (NM_001122987.1)	CACTGCTGAAGGAAGCCATC	GGGTCTTCATAGCCACAGGT
<i>PFKFB3</i> (XM_021065026.1)	GGACCGATGTTACCTTTGCC	TTGGCGTGGTTCAGTCTTTC
<i>PFKM</i> (DQ363336.1)	CGCTCCACTGTGAGAATTGG	GCTAAGCCCTCAAAGCCATC
<i>PFKP</i> (XM_021065066.1)	CCGACGGACACAAGATGTTC	TTGTCCCAAGAATGGAGCCT
<i>SLC37A4</i> (NM_001199719.1)	CTGTGGTCAGAAGCTCGTGT	GGAGAAGGTCCTGCGGTTGA
<i>G6PC1</i> (NM_001113445.1)	TTACCTGCTGCTAAAGGGGC	ACATGCTGGAGTTGAGAGCC
<i>PGM1</i> (NM_001246318.1)	CCTGTGGACGGAAGCATTTC	ATGTACAGTCGGATGGTGGC
<i>UGP2</i> (NM_213980.1)	GCAGTAGGGGCTGCCATTA	GCACGGTAGGAAATTCTCGC
<i>GYS1</i> (AJ507152.1)	TAGGCCGGGTATAACTCCCT	AAAGGGGCCGCAACCATTA
<i>PYGL</i> (NM_001123172.1)	CACCTGCATTCACACTGGTC	AGTAGTACTGCTGCGTGCG
<i>GAA</i> (XM_021066505.1)	CCTACACGCAGGTCGTCTTC	GTTGGAGACAGGAACACCGT
<i>G6PD</i> (XM_021080744.1)	GCGAGAAACTCCAGCCATT	GTAGGTGCCCTCGTACTGGA
<i>PGD</i> (XM_003127557.4)	TACTTCGGGGCTCACACCTA	GTACGAAGAGGAGGACACGC
<i>TKT</i> (NM_001112681.1)	GGGACAAGATAGCTACCCGC	TAGCACTCGATGAAGCGGTC
<i>TKTL1</i> (XM_021080741.1)	CTACCCAGAAGGTGGCATCG	GATGGACCAGGATGTCAGGC
<i>P2RY14</i> (XM_021069620.1)	CCACATTGCCAGAATCCCCT	CAGGCATACATTTGCAGCCG
<i>RARB</i> (XM_005669304.3)	CTCCGCAGCATCAGTGCTAA	TGGGGTCAAGGGTTCATGTC
<i>STAT1</i> (NM_213769.1)	CAAAGGAAGCCCCAGAACCT	CCCACCATTTCGAGACACCTC